Evaluation of the ^{13}N$(\alpha, p)\,^{16}$O thermonuclear reaction rate and its impact on the isotopic composition of supernova grains

A. Meyer,[1] N. de Séréville [ORCID],[1,*] A. M. Laird [ORCID],[2,3] F. Hammache [ORCID],[1] R. Longland [ORCID],[4,5] T. Lawson [ORCID],[6,7,3] M. Pignatari,[6,7,3,8] L. Audouin,[1] D. Beaumel,[1] S. Fortier,[1] J. Kiener,[9] A. Lefebvre-Schuhl,[9] M. G. Pellegriti,[1,10] M. Stanoiu,[11,12] and V. Tatischeff[9]

[1]*Institut de Physique Nucléaire d'Orsay, UMR8608, IN2P3-CNRS, Université Paris Sud 11, 91406 Orsay, France*
[2]*Department of Physics, University of York, York YO10 5DD, United Kingdom*
[3]*NuGrid Collaboration*
[4]*Department of Physics North Carolina State University, Raleigh, North Carolina 27695-8202, USA*
[5]*Triangle Universities Nuclear Laboratory, Durham, North Carolina, 27708-0308, USA*
[6]*E. A. Milne Centre for Astrophysics, Department of Physics and Mathematics, University of Hull,*
Kingston upon Hull HU6 7RX, United Kingdom
[7]*Konkoly Observatory, Research Centre for Astronomy and Earth Sciences, Hungarian Academy of Sciences, H-1121 Budapest, Hungary*
[8]*Joint Institute for Nuclear Astrophysics, Center for the Evolution of the Elements, Michigan State University,*
East Lansing, Michigan 48824, USA
[9]*Centre de Sciences Nucléaires et de Sciences de la Matière (CSNSM), CNRS/IN2P3 et Université Paris Sud 11, UMR 8609,*
Bâtiment 104, 91405 Orsay Campus, France
[10]*INFN-Sezione di Catania, via Santa Sofia 64 Catania, Italy*
[11]*GSI, Postfach 110552, D-64220 Darmstadt, Germany*
[12]*Horia Hulubei National Institute for Physics and Nuclear Engineering, P. O. Box MG-6, 077125 Bucharest-Măgurele, Romania*

Background: It has been recently suggested that hydrogen ingestion into the helium shell of massive stars could lead to high ^{13}C and ^{15}N excesses when the shock of a core-collapse supernova passes through its helium shell. This prediction questions the origin of extremely high ^{13}C and ^{15}N abundances observed in rare presolar SiC grains which is usually attributed to classical novae. In this context the ^{13}N$(\alpha, p)\,^{16}$O reaction plays an important role since it is in competition with ^{13}N β^+ decay to ^{13}C.

Purpose: The ^{13}N$(\alpha, p)\,^{16}$O reaction rate used in stellar evolution calculations comes from the Caughlan and Fowler compilation with very scarce information on the origin of this rate and with no associated uncertainty. The goal of this work is to provide a recommended ^{13}N$(\alpha, p)\,^{16}$O reaction rate, based on available experimental data, with a meaningful statistical uncertainty.

Method: Unbound nuclear states in the ^{17}F compound nucleus were studied using the spectroscopic information of the analog states in ^{17}O nucleus that were measured at the Tandem-Alto facility using the ^{13}C$(^7$Li, $t)\,^{17}$O α-particle-transfer reaction. The α-particle spectroscopic factors were derived using a finite-range distorted-wave Born approximation analysis. This spectroscopic information was used to calculate a recommended ^{13}N$(\alpha, p)\,^{16}$O reaction rate with meaningful uncertainty using a Monte Carlo approach.

Results: The ^{13}N$(\alpha, p)\,^{16}$O reaction rate from the present work is found to be within a factor of two of the previous evaluation in the temperature range of interest, with a typical uncertainty of a factor $\approx$2–3. The source of this uncertainty has been identified to come from the three main contributing resonances at $E_r^{\text{c.m.}} = 221$, 741, and 959 keV. This new error estimation translates to an overall uncertainty in the ^{13}C production of a factor of 50 when using the lower and upper reaction rates in the conditions relevant for the ^{13}N$(\alpha, p)\,^{16}$O activation.

Conclusions: The main source of uncertainty on the re-evaluated ^{13}N$(\alpha, p)\,^{16}$O reaction rate currently comes from the uncertain α-particle width of relevant ^{17}F states.

I. INTRODUCTION

Abundance measurements of isotopes and elements in stars provide a fundamental diagnostic for stellar evolution and internal stellar conditions. Theoretical predictions from stellar models can be directly compared with observations of very

───────────
*deserevi@ipno.in2p3.fr

old stars [1] or with evolved stars of any age including the Sun by using galactical chemical evolution simulations [2–4]. Specific information about individual stars and supernova explosions can be obtained, by, e.g., observing abundance signatures from supernova remnants [5,6] or by measuring abundances in single presolar grains found in meteorites. Presolar grains condensed around old dying stars like supernovae and asymptotic giant branch (AGB) stars just before

the formation of the Sun and then were trapped in meteorites formed in the early solar system. Pristine isotopic abundances in single presolar grains, therefore, carry the signature of their parent stars [7]. Isotopic ratios that are measured in single presolar grains can be used as a constraint to map stellar structure properties. Carbon-rich presolar grains from core-collapse supernovae provide fundamental insights about the supernova explosion, and about the progenitor massive star, specifically from the He-burning layers [7,8]. Data coming from presolar dust like SiC grains of Type X [9], Type C [10], and low-density graphites [11] challenge theoretical supernova models, highlighting their limitations and providing new puzzles to solve. Nuclear reaction rates relevant in these conditions are crucial ingredients of these models to define final stellar abundances.

Among the different types of presolar SiC grains, putative nova grains represented, for many years, an unsolved challenge for stellar models [12]. Nova grains show high excesses of isotopes ^{13}C and ^{15}N compared to the solar composition, that can be explained by the hot CNO cycle during typical nova conditions [13,14]. However, some of the nova grains also showed ^{44}Ca excess, which can only be explained as radiogenic contribution of the radioactive isotope ^{44}Ti. ^{44}Ti can be made in supernovae but not in novae, while standard supernova models were not able to explain the observed ^{13}C and ^{15}N abundances [12]. A realistic solution for this conundrum was provided in Ref. [15], using new supernova models where fresh hydrogen was ingested in the He-rich stellar layers of massive star progenitors, just before the supernova explosion. The nucleosynthesis obtained in the H-ingestion event, and the mixture of explosive He-burning and H-burning yields generated by the following supernova (SN) shock in the He-rich layers, provide the conditions to generate sufficient ^{13}C and ^{15}N abundances to explain measurements in putative nova grains. Typical temperatures ranging between 0.4 and 1 GK in the SN shock are achieved depending on the amount of H available in He-rich layers. However multidimensional hydrodynamics models are required to quantitatively study the stellar structure response and nucleosynthesis following H-ingestion events. While models of this kind exist for ingestion of H into the He shell in AGB stars, post-AGB stars and in rapidly accreting white dwarfs (WDs) (e.g., Refs. [16–18]), the first hydrodynamics simulations are only recently becoming available for massive stars [19]. For this reason, the nucleosynthesis analysis of Ref. [15] took into account different SN explosion energies and a large range of H concentration left after the ingestion. While a new generation of stellar models for massive stars informed from multidimensional hydrodynamics simulations are needed to drive more definitive conclusions, [15] showed that the production of ^{13}C and ^{15}N in He-rich layers consistent with the abundance pattern in putative nova grains is obtained for a wide combination of SN explosion energies and H concentration. In these models, during the SN explosion, the reaction ^{13}N(α, p)^{16}O is efficiently activated. ^{13}N is made by proton capture on ^{12}C. The accumulation of ^{13}N in the He shell will determine how much radiogenic ^{13}C will be ejected by the explosion. On the other hand, ^{13}N(α, p)^{16}O is depleting part of the ^{13}N made, producing instead ^{16}O.
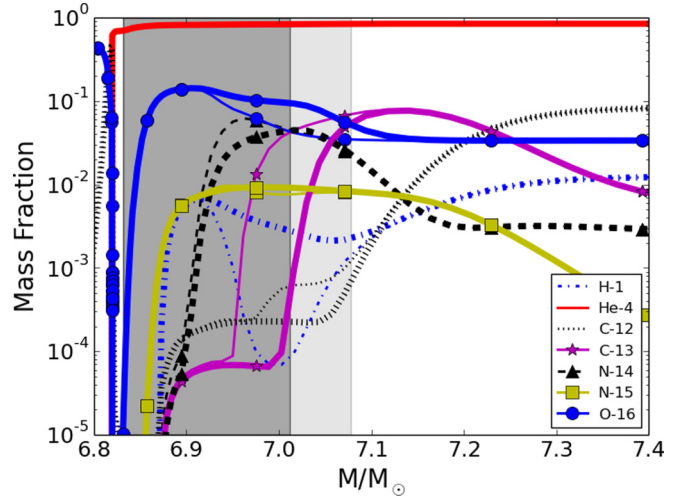

FIG. 1. Isotopic abundances in the He-shell ejecta of a 25 $M_\odot$ supernova model. Thick (thin) lines correspond to a ^{13}N(α, p)^{16}O reaction rate variation by a factor of five up (down), respectively. Shaded area identify the O-rich zones (or O-Nova zone, with C/O < 1) in the He shell region, where the dark grey (light gray) area is obtained by using the higher (lower) ^{13}N(α, p)^{16}O reaction rate.

The ^{13}N(α, p)^{16}O thermonuclear reaction rate used in stellar models [15] comes from the Caughlan and Fowler [20] (hereafter CF88) compilation. The impact of a variation of the ^{13}N(α, p)^{16}O reaction rate by an arbitrary factor of five with respect to the CF88 rate has been investigated and the results for decayed abundances are shown in Fig. 1, using the stellar simulations in Ref. [15]. The largest abundance variation is shown for H, ^{13}C, and ^{16}O, when the temperature peak of the SN shock is between 0.5 and 0.7 GK. A higher ^{13}N(α, p)^{16}O reaction rate destroys ^{13}N, producing more ^{16}O. Therefore, the abundance of ^{13}C, from the ^{13}N decay, decreases. The higher abundance of H is also due to a stronger activation of the (α, p) channel. Since the H reservoir is affected, the ^{13}N(α, p)^{16}O rate might potentially affect the efficiency of other proton capture reactions. In the final part of this work we will discuss this in more detail.

The thermonuclear ^{13}N(α, p)^{16}O reaction rate given in the CF88 compilation comes from the reverse ^{16}O(p, α)^{13}N reaction. However it is not clear from the CF88 compilation (and references therein) what is the origin of the nuclear data used to derive the ^{16}O(p, α)^{13}N reaction rate; moreover, no reaction rate uncertainty is given. A compilation of ^{16}O(p, α)^{13}N excitation functions can be found in Ref. [21] and some of the reported works [22,23] give reaction rates for temperatures $T_9 > 1.4$ [$T_9 \equiv T(K)/10^9$]. Unfortunately, this is higher than the temperature range of interest $T_9 = 0.4$–1 when the SN shock crosses the He shell. The first estimate of the thermonuclear ^{13}N(α, p)^{16}O reaction rate was given by Wagoner *et al.* [24,25] based on the formalism for nonresonant reactions [26], but no details are given on the origin of the numerical values used in the analytical formula of the reaction rate. Another estimate of the thermonuclear ^{13}N(α, p)^{16}O reaction rate based on the Hauser-Feshbach model can be found in the STARLIB library [27]. However, the use of such

a nuclear model for a low-mass-number ($A = 17$) nuclide with low level density is questionable and an uncertainty of a factor of 10 has been associated to the ^{13}N(α, p)^{16}O reaction rate [27]. Given this situation a re-evaluation of the thermonuclear ^{13}N(α, p)^{16}O reaction rate including a meaningful statistical uncertainty is necessary to constrain the effect of this rate on the final ^{13}C abundance.

The evaluation of the ^{13}N(α, p)^{16}O reaction rate in the temperature range of interest $T_9 = 0.4$–1 requires a detailed knowledge of the structure of the compound nucleus ^{17}F within around 2.5 MeV above the ^{13}N $+\alpha$ threshold. State energies are known though with a relatively large uncertainty of a few tens of keV [28]. Spins and parities are known in most cases and the total widths are known experimentally [28]. Given that the ^{13}N $+\alpha$ threshold [$S_{\alpha+^{13}N} = 5818.7$ (4) keV] is much higher than the ^{16}O $+p$ threshold [$S_p = 600.27$ (25) keV], the states in the region of interest decay mainly by proton emission, so that $\Gamma_p \approx \Gamma_{tot}$. Their contribution to the reaction rate is therefore directly proportional to their unknown α-particle widths. This paper provides an evaluation of the α-particle widths of ^{17}F states based on the properties of ^{17}O analog states when a pairing connection exists.

The goal of this work is to determine statistically meaningful thermonuclear rates for the ^{13}N(α, p)^{16}O reaction. Unfortunately a direct measurement of this reaction cross section is not currently feasible with existing ^{13}N beam intensity, and therefore we rely on an indirect approach. We first report on the analysis of ^{13}C(^{7}Li, t)^{17}O α-particle transfer reaction measurement in order to determine the α-particle spectroscopic factors of ^{17}O analog states of ^{17}F (Sec. II). Under the mirror symmetry assumption, spectroscopic information for the analog ^{17}F states is then derived (Sec. III) and further used to evaluate thermonuclear rates and rate uncertainties (Sec. IV). Finally, the impact of the new ^{13}N(α, p)^{16}O reaction rate in the hydrogen ingestion scenario in massive stars is explored (Sec. V).

II. STUDY OF THE ^{13}C(^{7}Li, t)^{17}O TRANSFER REACTION

A. Experimental procedure

The ^{13}C(^{7}Li, t)^{17}O reaction measurement [29] was performed at the Tandem-ALTO facility in Orsay, France. Experimental details can be found in Ref. [29] and the most relevant information for the present study is recalled here. A ^{7}Li^{3+} beam of about 100 enA was accelerated by the 15-MV Tandem to an energy of 34 MeV. The beam impinged on a self-supporting enriched (90%) ^{13}C target of 80(4) μg/cm^2 located at the object focal plane of an Enge Split-Pole magnetic spectrometer [30]. Light reaction products were momentum analyzed and focused on the focal-plane detection system [31], and tritons were readily distinguished from deuterons using the energy loss and magnetic rigidity measurements. The tritons were detected at 11 angles between 0° and 33° in the laboratory frame. The unreacted beam was detected inside the reaction chamber by a Faraday cup at 0° recording the accumulated charge of each run.

B. Data reduction

After selection, triton spectra of the focal-plane position were obtained for each spectrometer angle and the case of
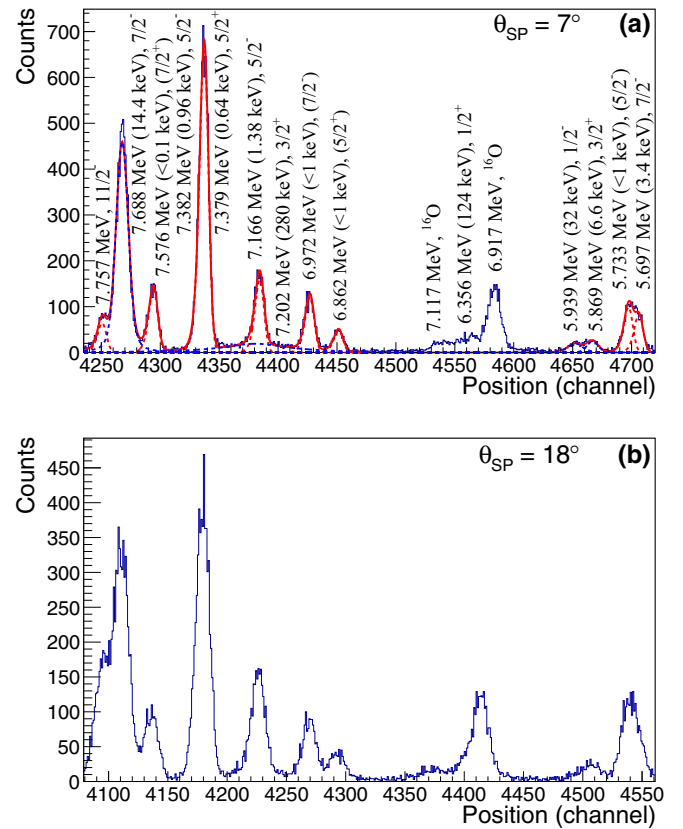

FIG. 2. Triton magnetic rigidity spectrum at spectrometer angle of 7° and 18° corresponding to an incident charge of 585 and 1155 μC, respectively. Excitation energies in ^{17}O between 5.6 and 7.8 MeV are covered. All triton peaks correspond to known ^{17}O states unless this is indicated. For the data at 7°, the best fit of the spectrum is shown (solid line), together with individual contributions (dashed lines) for narrow states (red) and states with known widths (blue). Labeled energies, total widths, and spin parities are from the last National Nuclear Data Centre (NNDC) compilation [28], except for the broad state at 7.202 keV whose width is from the present analysis.

7° and 18° are shown in Fig. 2. Apart from the two triton contamination peaks associated to ^{16}O states at 6.917 and 7.117 MeV, all peaks could be identified with known ^{17}O states. This identification relies on two considerations: the use of the focal-plane detector calibration and the kinematics of the ^{13}C(^{7}Li, t)^{17}O reaction.

The calibration of the focal-plane detector was performed using a ^{nat}C target and narrow well-isolated ^{16}O states populated from the ^{12}C(^{7}Li, t)^{16}O reaction. The relation between the radius of curvature and the focal-plane position was obtained and the calibration deduced after fitting this relation by a one-degree polynomial function. The calibration was then applied to the raw data and the magnetic rigidity of the observed triton peaks matched the expectation from the energy of ^{16}O states.

Comparison of the triton peaks at the spectrometer angles of 7° and 18° shows that the relative position of the peaks is the same. This behavior confirms that the triton peaks correspond to excited states belonging to the same nucleus. It was checked that the experimental difference of magnetic
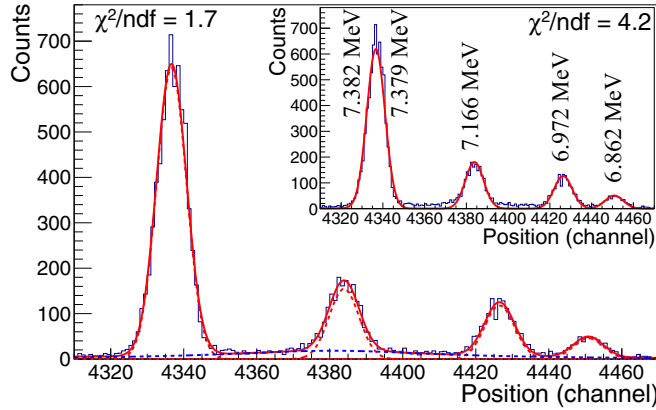
FIG. 3. Triton magnetic rigidity spectrum at spectrometer angle of 7° zoomed in the ^{17}O excitation energy region between 6.8 and 7.4 MeV. The broad ^{17}O state at 7.202 MeV is included in the fitting procedure and its contribution is represented by the dashed blue line. The insert shows a fit of the same data without the inclusion of the broad state. Reduced chi squares are also given.

rigidity between angles for a same state was following the ^{13}C(^{7}Li, t)^{17}O kinematics. This again supports the identification of triton peaks as ^{17}O excited states. Any two-body reaction occurring on nuclei different from ^{13}C (e.g., contaminants in the target) will produce triton peaks that will have a different kinematic dependence than ^{17}O states. This is the case for the peaks associated to ^{16}O states at 6.917 and 7.117 MeV, which are moving toward the ^{17}O state at 6.862 MeV as the detection angle is increasing.

The triton magnetic rigidity spectra were independently analyzed using a least-squares fit of multiple Gaussian and Voigt functions at each detection angle, and the best fit was obtained. The Gaussian function was used to describe ^{17}O states having natural widths much smaller than the experimental resolution of ≈50 keV (full width at half maximum, center of mass). A common width was used as a free parameter in the fitting procedure. The Voigt function was used to describe triton peaks associated to ^{17}O states at 5.697, 5.869, 5.939, 7.202, and 7.688 MeV, which have a sizable total width. The natural width was kept as a fixed parameter in the Lorentzian component of the Voigt function while the width of the Gaussian component was the same free parameter as for the Gaussian used to describe the narrow states. The natural width of the ^{17}O state at 7.202 MeV was determined from the present data (see below). The magnetic rigidity region around the ^{17}O state at 6.356 MeV and the two ^{16}O contamination states were excluded from our fitting procedure since results concerning this energy region have already been reported [29]. The best fit of the triton magnetic rigidity spectrum obtained at a spectrometer angle of 7° is represented in Fig. 2. The states at 5.697 and 5.733 MeV were not included in the fitting procedure for the higher detection angle because they were hindered by an ^{16}O contamination state.

A close-up of the excitation energy region between 6.8 and 7.4 MeV is shown in Fig. 3 where the contribution of the ^{17}O state at 7.202 MeV is represented by dashed blue line. The insert in Fig. 3 corresponds to the fitting case when the broad

state is not taken into account. The reduced chi square is much better when the broad state is included (χ^2/ndf = 1.7) than without broad state (χ^2/ndf = 4.2), which strongly supports the observation of the 7.202 MeV state in the present data. Several values of the total width of the broad ^{17}O state at 7.202 MeV can be found in the literature, ranging from 280 (30) keV [28,32] to 400 (30) keV [33], while a recent measurement reports 262 (7) keV [34]. The natural width of the 7.202 MeV state was therefore kept as a free parameter in the fitting procedure described above and a value of 313 (22) keV was found after averaging over the first eight smaller spectrometer angles. Our result agrees within 1-σ with the adopted value from Refs. [28,32] and within 2-σ with the two other values available in the literature [33,34].

C. Angular distributions and DWBA analysis

The differential cross sections corresponding to populated ^{17}O states were calculated from the triton yield determined at each spectrometer angle $Y_t(\theta_{\text{lab}})$ using the following formula:

$$\left(\frac{d\sigma}{d\Omega}\right)_{\text{c.m.}} (\theta_{\text{c.m.}}) = \frac{Y_t(\theta_{\text{lab}})}{Q(\theta_{\text{lab}})N_{\text{target}}\Delta\Omega_{\text{lab}}} J(\theta_{\text{lab}}), \quad (1)$$

where $Q(\theta_{\text{lab}})$ is the accumulated charge at each angle, N_{target} is the number of ^{13}C atoms per unit area, $\Delta\Omega_{\text{lab}}$ is the Split-Pole solid angle, and $J(\theta_{\text{lab}})$ is the Jacobian for the laboratory to center-of-mass transformation of the ^{13}C(^{7}Li, t)^{17}O reaction at each spectrometer angle. The differential cross sections are shown in Fig. 4 together with finite-range distorted-wave Born approximation (FR-DWBA) calculations performed with the FRESCO code [35].

We follow the prescription from Ref. [29] for the choice of optical potential parameters and for the overlap between the $\alpha + t$ and ^{7}Li systems. Several combinations of entrance and exit optical potential parameters have been tested as inputs of the DWBA calculations [36]. The best compromise for describing differential cross sections for all ^{17}O states at the same time was obtained with the potential III from Ref. [37] for the ^{13}C + ^{7}Li entrance channel and with the potential I.a from Ref. [38] for the $t + ^{17}$O exit channel. Concerning the α-wave function in ^{17}O, the depth of a Woods-Saxon potential ($r = 4$ fm and $a = 0.76$ fm) was adjusted to reproduce the known α-separation energy for each state. The number of radial nodes N (including the origin) of the α-wave function in ^{17}O was set using the usual oscillator energy conservation rule [39] when the number of quanta in the relative motion $Q = 2(N-1) + L$ is equal to 6 for negative-parity states and 7 for positive-parity states. This can be linked to 2p-1h and 3p-2h shell model configurations for negative- and positive-parity states, respectively, as suggested by theoretical calculations [40] for ^{17}O states of high excitation energies. Note that the shape of the angular distribution calculated by the DWBA model shows very little sensitivity to the number of nodes N. In the case of negative-parity states we indeed considered calculations with $Q = 8$ which could be associated to the possible 4p-3h configuration, and as expected the shape of the calculated angular distributions were very similar though the $Q = 6$ case slightly better described the data.
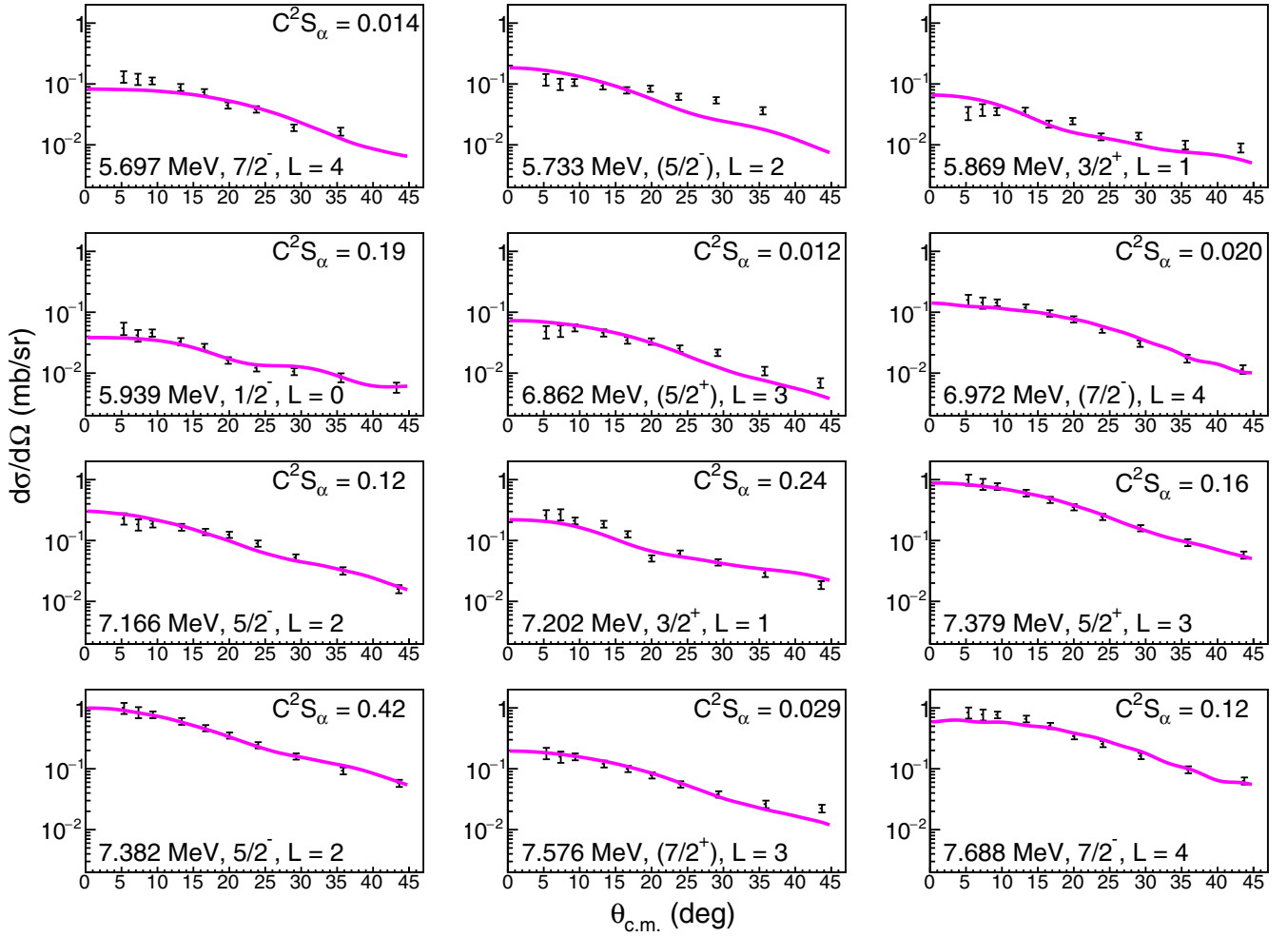
FIG. 4. Experimental differential cross sections of ^{17}O states populated with the ^{13}C(^{7}Li, t) ^{17}O reaction at 34 MeV. Solid lines represent finite-range DWBA calculations normalized to the data.

As can be seen in Fig. 4 a very good agreement is observed between normalized FR-DWBA calculations and the data in most cases. This supports a single step direct mechanism for the population of ^{17}O states using the ^{13}C(^{7}Li, t) ^{17}O reaction; the only exception being for the two ^{17}O states at 5.733 and 5.869 MeV. This is not surprising since their experimental differential cross sections vary less strongly as a function of the center-of-mass angle, which suggests that these states are significantly populated by the triton evaporation of the compound nucleus ^{20}F or by a multiple step reaction mechanism.

The normalization factor between the experimental and DWBA differential cross sections for a given state is equal to the product of the ^{17}O α-particle spectroscopic factor (C^2S_α) and the square of the overlap between the $\alpha + t$ and ^{7}Li systems ($S_\alpha^{7\text{Li}}$). We used $S_\alpha^{7\text{Li}} = 1$ in the present work following the prescription from Ref. [29]. Determination of α-particle spectroscopic factors for unbound ^{17}O states follows the prescription given in Ref. [41]. The calculation of the α-wave function for unbound ^{17}O states used form factors obtained with the α-cluster bound at 0.1 MeV. This should be suitable for states associated to large transferred angular momentum ($L \geqslant 2$) since the α-cluster is quasibound due to the large centrifugal barrier. In case of lower transferred

angular momentum such as for the ^{17}O state at 7.202 MeV ($L = 1$) the calculation was performed at several α-binding energies approaching zero and the DWBA cross section was extrapolated to the actual α-separation energy (see Fig. 3 in Ref. [36] for an example).

For unbound states the α-particle partial width can be deduced from the corresponding spectroscopic factor using the following formula [42]

$$\Gamma_\alpha = 2P_L(r, E)\frac{\hbar^2 r}{2\mu}C^2S_\alpha \,|\phi(r)|^2, \qquad (2)$$

where μ is the reduced mass for the $\alpha + ^{13}$C system, $P_L(r, E)$ is the penetrability of the Coulomb and centrifugal barriers for transferred angular momentum L, and $|\phi(r)|$ is the radial part of the $\alpha + ^{13}$C wave function. Equation (2) has been evaluated at the interaction radius $r = 7.5$ fm where the $\alpha + ^{13}$C wave function reaches an asymptotic behavior [36].

The parameters used in the FR-DWBA analysis and the results from the present work are presented in Table I. Comparison with α-particle widths determined from previous experimental work reported in the last NNDC compilation [28] is also provided. A very good agreement is found between

TABLE I. Alpha-particle spectroscopic factors and widths for ^{17}O states obtained from the present analysis. Comparison with α widths from the literature is provided.

NNDC [28]			Present work			Heil *et al.* [43]		Sayer *et al.* [44]	
E_x (keV)	J^π	Γ_α (keV)	N, L^a	$C^2 S_\alpha$	$\Gamma_\alpha^{\ b}$ (keV)	E_x (keV)	Γ_α (keV)	E_x (keV)	Γ_α (keV)
5697.3 (4)	$7/2^-$		2, 4	0.014		5696.7	2.4×10^{-11}	5696.7	
5732.8 (5)	$(5/2^-)$		3, 2			5733.5	4.1×10^{-9}	5732.3	
5869.1 (6)	$3/2^+$		4, 1			5868.4	-4.1×10^{-4}	5868.7	
5939 (4)	$1/2^-$		4, 0	0.19		5923.2	5.5×10^{-9}	5932.0	
6356 (8)	$1/2^+$		4, 1	0.29^c	13.5 ± 6.6^c	6379.5	1.7×10^{-54}	6380.2	
6862 (2)	$(5/2^+)$		3, 3	0.012	1.1×10^{-7}	6829.8	1.1×10^{-6}	6860.7	
6972 (2)	$(7/2^-)$		2, 4	0.020	8.2×10^{-8}	6936.2	3.3×10^{-6}	6971.9	
7165.7 (8)	$5/2^-$	0.0033	3, 2	0.12	3.4×10^{-3}	7164.6	4.3×10^{-3}	7164.6	0.009
7202 (10)	$3/2^+$	0.07	4, 1	0.24	7.3×10^{-2}	7247.7	0.14	7239.1	0.17
7379.2 (10)	$5/2^+$	0.01	3, 3	0.16^d	8.0×10^{-3}	7377.9	0.011	7378.2	0.02
7382.2 (10)	$5/2^-$	0.003	3, 2	0.42^d	0.131	7380.7	2.9×10^{-3}	7380.8	0.007
7559 (20)	$3/2^-$	0.08				7475.2	0.027	7446.9	0.026
7576 (2)	$(7/2^+)$		3, 3	0.029	7.3×10^{-3}				
7688.2 (9)	$7/2^-$	0.01	2, 4	0.12	3.3×10^{-3}	7686.0	0.011	7686.9	0.026

[a]The quantities N and L are the radial nodes (including the origin) and orbital angular momentum assigned to the center-of-mass motion of the α cluster in ^{17}O.

[b]$\Gamma_\alpha = 2P_l(a, E)\frac{\hbar^2 a}{2\mu}C^2 S_\alpha |\phi(a)|^2$ with $|\phi(a)|$ being the radial part of the ^{13}C $+ \alpha$ wave function evaluated at the channel radius $a = 7.5$ fm (see text).

[c]From Ref. [29], the reduced width γ_α^2 is given instead of Γ_α.

[d]This doublet is not resolved experimentally so the deduced spectroscopic factor assumes all the strength is on one or the other state.

our results and the literature, typically within a factor of two. The only noticeable difference is for the ^{17}O state at 7382.2 keV which is part of an unresolved doublet with the 7379.2-keV state in the present experiment. If we assume that all the strength is on the 7379.2-keV state, then we find an α-particle width in very good agreement with NNDC [28]. On the other hand, if we assume that all the strength is on the 7382.2-keV state, then our determination of the α-particle width is about 50 times larger than the one reported in NNDC [28]. This indicates most probably that the ^{17}O state at 7379.2 keV has been preferentially populated in the present experiment.

Comparison with α-particle widths determined from works using $\mathcal{R}$-matrix analysis of the ^{13}C(α, n) ^{16}O reaction [43,44] is also provided in Table I. A good agreement is obtained for excitation energies greater than 7 MeV with the exception of the ^{17}O state at 7382.2 keV as explained before. Below 7 MeV there is no ^{13}C $+\alpha$ experimental data which can be used to constrain the α-particle widths of ^{17}O states. This explains the difference between our results and those of Ref. [43] which come from an extrapolation of the cross section measured at higher energies.

III. RESONANCE PARAMETERS IN ^{17}F

For temperatures achieved during explosive burning in the He shell of massive stars ($T_9 = 0.4 - 1$) the energy range of the Gamow window for the ^{13}N(α, p) ^{16}O reaction corresponds to excitation energies of ^{17}F between 6.22 and 7.20 MeV. Four ^{17}F states are known in this energy region (see Fig. 5), but the tails of broad states lying above the Gamow

window could also contribute to the reaction rate. Hence, in the following, we consider ^{17}F states having excitation energies up to 8.2 MeV and the relevant spectroscopic information is presented in Table II.

States in ^{17}F above the $\alpha + ^{13}$N threshold ($S_{\alpha + ^{13}\text{N}} = 5818.7$ (4) keV [28]) have mainly been studied by the ^{16}O(p, p) ^{16}O reaction [45,46] and by the ^{16}O(p, p') ^{16}O and ^{16}O(p, α) ^{13}N reactions [47]. These experiments measured excitation functions and were performed by the same group using the University of Wisconsin tandem Van de Graaff installation. Spin, parity, total width, and energy of the ^{17}F states were determined. Energies of the ^{17}F states were derived from the incident proton beam energy assuming a proton separation energy value ($S_p = 596$ keV [46,47]) which is now superseded ($S_p = 600.27$ (25) keV [48]). This information was not updated in the last NNDC compilation [28] but has been taken into account in Table II. The large reported uncertainty (≈ 20 keV) associated to the energy of most of the ^{17}F states (see Table II) comes from a possible error in the calibration of one of the magnets in the beam line [49]. The excitation energy uncertainty should therefore be better considered as a systematic error rather than a statistical uncertainty. No uncertainty is reported for the energy of the state at 8.224 MeV although it was observed jointly with the states at 7.753 and 8.073 MeV [47] for which uncertainties were given. Due to the large width of the 8.224-MeV state [$\Gamma = 706$ (235) keV], and based on the reported energy uncertainties in this excitation energy region [28], we assign an uncertainty of 40 keV to its excitation energy.

Excitation energies are then used to derive resonance energies using the relation $E_r = E_x - S_{\alpha + ^{13}\text{N}}$, and the uncertainty
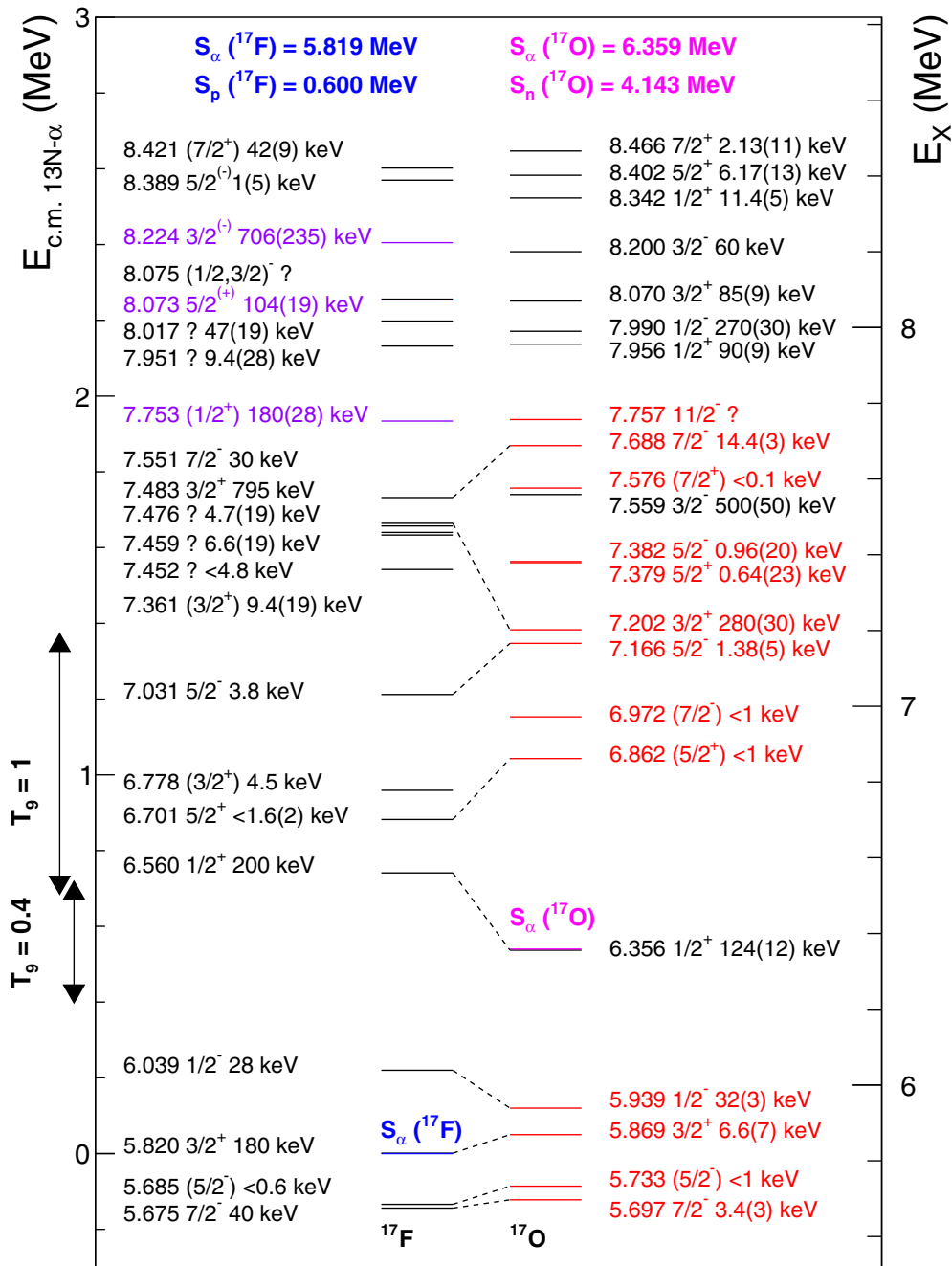
FIG. 5. Level scheme of ^{17}F nucleus above the $\alpha + ^{13}$N threshold and comparison with its mirror nucleus ^{17}O. Mirror pairs are linked with dashed lines. ^{17}O states studied in the present analysis are in red. ^{17}F states in purple have experimentally determined partial and total widths. Black arrows indicate the energy range of the Gamow window for two temperatures of interest.

associated to the resonance energy is dominated by the one on excitation energies.

For the ^{17}F states under study there is neither experimental determination nor theoretical estimate of their partial widths (Γ_p and Γ_α), except for the three broad states at 7.753, 8.073, and 8.224 MeV. The reduced widths (γ_i^2) of these three broad resonances are reported for the p_0, p_1, and α_0 channels [47] and this information was used to calculate the partial widths reported in Table II. In the case of the 7.753-MeV state two partial widths sets are reported [47]: (Γ_α, Γ_{p_0}, Γ_{p_1}) =

(11 keV, 135 keV, 34 keV) and (34 keV, 41 keV, 109 keV). Both sets give similar results for the contribution of the 7.753-MeV state since the total width and its energy dependence are very similar in both cases. We therefore arbitrary choose set 1 (reported in Table II) for the partial widths of the 7.753-MeV state.

For the other ^{17}F states with no experimental determination of their partial widths, they need to be estimated and two different cases are considered depending on the existence of a known analog state in ^{17}O.

TABLE II. Resonance parameters in ^{17}F above ^{13}N $+\alpha$ threshold [$S_{\alpha+^{13}\mathrm{N}} = 5818.7\,(4)$ keV] and spectroscopic information for the ^{17}O analog states when available. ^{17}O state properties come from NNDC [28] unless otherwise stated.

^{17}F								^{17}O				
E_x [a] (MeV)	E_r (keV)	J^π	ℓ_α, ℓ_p	Γ_α [b] (keV)	Γ_{p_0} [c] (keV)	Γ_{p_1} (keV)	Γ_{tot} [d] (keV)	E_x (MeV)	J^π	Γ_α (keV)	Γ_n (keV)	Γ_{tot} (keV)
5.820 (20)	1.3	$3/2^+$	1, 2	6.92×10^{-28} [3h]	180		180	5.869	$3/2^+$		6.6	6.6 (7)
6.039 (9)	221	$1/2^-$	0, 1	2.63×10^{-13}	28		28	5.939	$1/2^-$		31.5	32 (3)
6.560 (20)	741	$1/2^+$	1, 0	1.88×10^{-3}	200		200	6.356	$1/2^+$		124	124 (12)
6.701 (7)	882	$5/2^+$	3, 2	1.76×10^{-5}	1.6		$\leqslant 1.6$ (2)	6.862	$(5/2^+)$			< 1
6.778 (20)	959	$(3/2^+)$	1, 2	3.00×10^{-2}	4.47		4.5					
7.031 (20)	1213	$5/2^-$	2, 3	3.59×10^{-2}	3.76		3.8	7.166	$5/2^-$	0.0033	1.38 (5)	1.38 (5)
7.361 (20)	1542	$(3/2^+)$	1, 2	2.20	7.20		9.4 (19)					
7.452 (20)	1633						$\leqslant 4.7$					
7.459 (20)	1640						6.6 (19)					
7.476 (20)	1657						4.7 (19)					
7.483 (20)	1664	$3/2^+$	1, 2	4.64	790.36		795	7.202	$3/2^+$	0.07	280	280 (30)
7.551 (20)	1732	$7/2^-$	4, 3	1.10×10^{-2}	29.98		30	7.688	$7/2^-$	0.01	13.0 (6)	14.4 (3)
7.753 (40)	1935	$(1/2^+)$[e]	1, 0	11 [f]	135 [f]	34 [f]	180 (28)	7.956	$1/2^+$	6.7	84	90 (9)
7.951 (30)	2132						9.4 (28)					
8.017 (40)	2198						47 (19)					
8.073 (30)	2255	$5/2^{(+)}$[e]	3, 2	14 [f]	79 [f]	11 [f]	104 (19)					
8.075 (10)	2256	$(1/2, 3/2)^-$	0-2, 1									
8.224 (40)[g]	2405	$3/2^{(-)}$[e]	2, 1	25 [f]	636 [f]	45 [f]	706 (235)					

[a] Energies have been corrected when needed with the new ^{16}O $+p$ threshold value ($S_p = 600.27$ keV [48]), see text. Uncertainties are from the latest compilation [28]. Note that reported uncertainties greater than 10 keV used to be smaller by a factor of two (see footnote *a* in Table 17.19 [49].)

[b] When a mirror connection exists the same reduced width γ_α^2 is assumed between analog states. Otherwise a dimensionless reduced width $\langle\theta_\alpha^2\rangle = 0.04$ is assumed [52,53]. In all cases a channel radius of 7.5 fm is used.

[c] $\Gamma_{p_0} = \Gamma_{\mathrm{tot}} - \Gamma_\alpha$.

[d] Total widths have been transformed to center-of-mass values when needed.

[e] While parity for these three states is uncertain, their relative ordering is fixed [47].

[f] Γ_{p_0}, Γ_{p_1}, and Γ_α are deduced from reduced widths derived from ^{16}O(p, p) ^{16}O [45,46] and ^{16}O(p, p') ^{16}O and ^{16}O(p, α) ^{13}N [47] measurements.

[g] Uncertainty is set arbitrarily from present work (see text).

[h] Despite an established mirror connection, a dimensionless reduced width $\langle\theta_\alpha^2\rangle = 0.04$ is assumed since the α spectroscopic factor for the $E_x = 5.869$ MeV state in ^{17}O could not be determined (see text).

Pairing of analog states between the ^{17}F and ^{17}O nuclei was based on their spin and parity information and the consistency of their partial and total widths. Identified analog states from the present work are connected by dashed lines in Fig. 5. For these states we assume that mirror symmetry holds and that $C^2 S_\alpha(^{17}\mathrm{F}) = C^2 S_\alpha(^{17}\mathrm{O})$ [50]. The α-particle partial width of ^{17}F states is then calculated using Eq. (2) where the reduced mass and penetrability quantities refer to the $\alpha + {}^{13}$N system instead. Note that there are some indication of possible charge-symmetry breaking in the lower part of the ^{17}F-^{17}O level scheme [51].

For ^{17}F states with no spectroscopic information and no identified analog state their α-particle partial width must be estimated. In this case the α width can be calculated using the following formula [42]:

$$\Gamma_\alpha = \theta_\alpha^2 \times \Gamma_\alpha^{\mathrm{Wigner}}, \qquad (3)$$

where θ_α^2 is the dimensionless reduced α-particle width and $\Gamma_\alpha^{\mathrm{Wigner}} = 2\hbar^2/(\mu r^2) \times P_L(r, E)$ is the Wigner limit. We used a mean reduced α-particle width of $\langle\theta_\alpha^2\rangle = 0.04$ following the

same approach as in Ref. [52]. This value was obtained from an extrapolation of a data set providing mean dimensionless α-particle reduced widths from nuclei having slightly larger mass numbers A [53].

For all determinations of the ^{17}F α-particle partial widths in the present work we use the same channel radius $r = 7.5$ fm as for the determination of $\Gamma_\alpha(^{17}\mathrm{O})$, which corresponds to $r_0 = 1.9$ fm, where r_0 is defined as $r = r_0 \times (A_\alpha^{1/3} + A_{^{13}\mathrm{N}}^{1/3})$. Proton widths are deduced in all cases as $\Gamma_p = \Gamma_{\mathrm{tot}} - \Gamma_\alpha$, except in the case of the three broad states at 7.753, 8.073, and 8.224 MeV. The ^{17}F resonance parameters derived from this work are summarized in Table II, and spectroscopic information of ^{17}O states is given when pairing of analog states is established.

The contribution of individual ^{17}F resonances to the astrophysical S-factor $S(E)$ of the ^{13}N(α, p) ^{16}O reaction, calculated using the spectroscopic information given in Table II, is shown in Fig. 6(a). Calculations were performed with the $\mathcal{R}$-matrix code AZURE2 [54] using channel radius $r_\alpha = 7.5$ fm and $r_p = 6.7$ fm. Solid lines correspond to resonances for which the α-particle partial width is estimated from
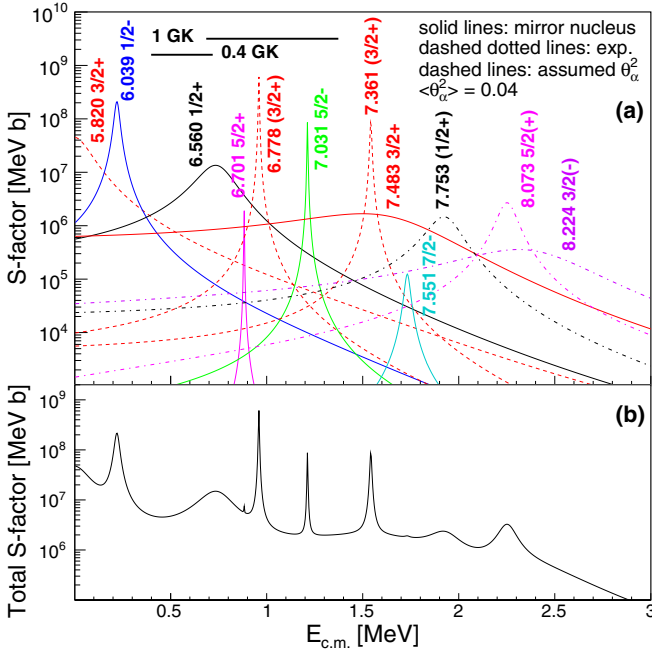
FIG. 6. Astrophysical S-factor for the ^{13}N(α, p) ^{16}O reaction as a function of the center-of-mass energy. $\mathcal{R}$-matrix calculations using the AZURE2 code with the parameters given in Table II are represented for individual resonances in panel (a). The Gamow energy window is represented for the temperatures $T_9 = 0.4$ and $T_9 = 1$. Panel (b) represents the total astrophysical S-factor when individual contributions from panel (a) are summed.

the analog states, and dashed lines correspond to resonances where $\langle \theta_\alpha^2 \rangle = 0.04$ is assumed. The major contribution to the S-factor in the temperature range of interest comes from the broad $E_r = 741$ keV and the two narrow $E_r = 959$ and 1213 keV resonances corresponding to low ℓ_α angular momentum. Resonances lying outside the Gamow window have a minor contribution in the energy region of interest, except in case of the broad $E_r = 1664$ keV resonance for the highest temperatures ($T_9 = 1 - 2$). The total astrophysical S-factor obtained when all individual contributions are summed is shown in Fig. 6(b).

IV. MONTE CARLO REACTION RATES

A. Method

The reaction rate per particle pair is defined as [42]

$$\langle \sigma v \rangle = \left(\frac{8}{\pi \mu} \right)^{1/2} \frac{1}{(kT)^{3/2}} \int_0^\infty E \sigma(E) e^{-E/kT} dE, \quad (4)$$

where μ is the reduced mass of the interacting particles, k is the Maxwell-Boltzmann constant, T is the temperature, and $\sigma(E)$ is the nuclear reaction cross section. In the present case the ^{13}N(α, p) ^{16}O reaction proceeds through several resonances and the cross section associated to a single resonance is defined by the one-level Breit-Wigner formula

$$\sigma(E) = \frac{\lambda^2}{4\pi} \frac{(2J + 1)}{4} \frac{\Gamma_\alpha(E) \Gamma_p(E + Q)}{(E - E_r)^2 + \Gamma/4}, \quad (5)$$

where λ is the de Broglie wavelength; J and E_r are the spin and energy of the ^{17}F resonance, respectively; Γ_i are the energy dependent partial widths and Γ is the total width.

In order to determine a statistically meaningful ^{13}N(α, p) ^{16}O reaction rate the Monte Carlo method developed by Ref. [55] has been followed. In summary, the energy and partial widths of each resonance are varied according to the probability density function defined by the experimental mean value and the associated uncertainty. For a given variation of the resonance energy, the partial widths are consistently evaluated by using the correct energy in the determination of the penetrability of the Coulomb and centrifugal barriers. For each Monte Carlo realization, all uncertain resonance parameters are sampled and a reaction rate is calculated. For a sufficiently large number of realizations (10 000 in the present work), a statistical meaningful recommended, low and high reaction rates can be defined. They are defined in this work as the 50th, 16th, and 84th percentile of the cumulative rate distribution, respectively.

Two different probability density functions are used for sampling the α-particle width of ^{17}F states depending on whether or not an analog ^{17}O state is known. When this is known, a lognormal distribution is used and an uncertainty of a factor of 2.5 on the α-particle particle width is assumed. This uncertainty comes from the combination of the uncertainty on the ^{17}O α-particle spectroscopic factor deduced from the transfer reaction ($\approx 50\%$) and the assumption of mirror symmetry which accounts for a factor of two uncertainty when states with relatively large spectroscopic factors are considered [52]. In case of ^{17}F states with no identified analog state, the α width is sampled according to a Porter-Thomas distribution of dimensionless reduced α-particle width $\langle \theta_\alpha^2 \rangle = 0.04 \pm 0.02$.

Concerning the proton width of ^{17}F states a lognormal distribution is used and an uncertainty of 20% is assumed when no such uncertainty is reported in the literature. In the case of the three broad states measured directly we estimate an uncertainty for their α-particle and proton widths assuming the same relative uncertainty as for their total width.

For the resonance energies we assume a Gaussian probability density function. Usually, energy uncertainties are considered independent from each others, which is a valid assumption when energy determination comes from different experimental techniques where systematic uncertainties are expected to be uncorrelated. In the present case, however, all states having energy uncertainties greater than 20 keV have been studied by the same group at the same facility using the same experimental technique, which leads to highly correlated uncertainties (see Sec. III). Here we extend the Monte Carlo method by implementing correlated energy uncertainties for several resonances following a similar approach as for the correlated uncertainties on resonance strengths [56]. First, the smallest energy uncertainty is identified (20 keV in the present case), and then the ratio of this value to each individual resonance energy uncertainty, σ_{Ej}, is used to calculate a correlation factor, ρ_j. Two cases are considered: (i) a resonance with an uncertainty equal to the 20-keV minimum uncertainty in the present case (for this resonance, $\rho = 1$) and (ii) a resonance with a much larger uncertainty, say,
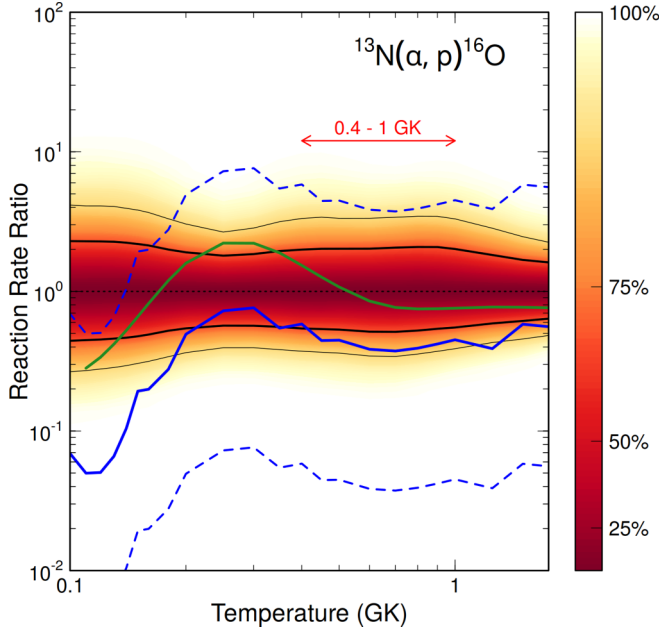
FIG. 7. Ratio of different ^{13}N$(\alpha, p)^{16}$O reaction rates normalized to the recommended reaction rate defined as the 50th percentile of the cumulative rate distribution obtained from the Monte Carlo procedure. The area delimited by the thick/thin black lines comprise a coverage probability of 68%/95%, respectively. The green line corresponds to the ^{13}N$(\alpha, p)^{16}$O reaction rate given by CF88, while the blue lines represent the nominal ^{13}N$(\alpha, p)^{16}$O reaction rate with associated uncertainty from STARLIB.
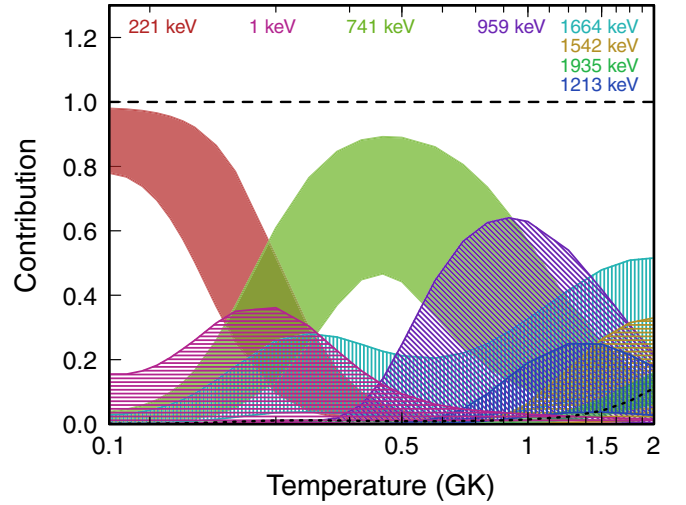

FIG. 8. Fractional contribution of individual resonances to the ^{13}N$(\alpha, p)^{16}$O reaction rate. The numbers at the top of the figure correspond to the center-of-mass energy of each resonance.

40 keV, yielding $\rho = 20/40 = 0.5$. During the Monte Carlo procedure, each resonance energy sample, $E_{j,i}$, for resonance j is computed using the following procedure. A reference sample, $x_{r,i}$, and uncorrelated samples for each resonance, $y_{j,i}$, are obtained from a Normal distribution (that is, a Gaussian distribution with a mean, $\mu = 0$, and standard deviation, $\sigma = 1$). Correlated, normally distributed random samples for each resonance are then calculated using:

$$y'_{j,i} = \rho_j x_{r,i} + \sqrt{1 - \rho_j^2} y_{j,i}. \qquad (6)$$

Finally, the resonance energy samples are calculated using

$$E_{j,i} = E_j + \sigma_{Ej} y'_{j,i}. \qquad (7)$$

For ^{17}F states where spin and parity assignments are uncertain, a range of possible J^π defined by $\ell_\alpha \pm 1$ is considered, where ℓ_α is the tentative α-particle orbital angular momentum given in Table II. This range is then sampled according to a discrete probability density function for each Monte Carlo realization. Following the approach of Mohr *et al.* [52] a probability of 50% is taken for the tentative spin and parity while the remaining 50% are equally shared between the other spin and parity possibilities.

B. ^{13}N$(\alpha, p)^{16}$O reaction rate

The results of the Monte Carlo simulation for the ^{13}N$(\alpha, p)^{16}$O reaction rates are presented in Fig. 7, where all rates are normalized to the recommended reaction rate defined

in the previous section. The colored area represents a coverage probability of 68% which corresponds to an uncertainty of a factor of about two to three at the temperature of interest $T_9 = 0.4$–1. This is not surprising since the reaction rate in this temperature range is dominated by the contribution of the 221- and 741-keV resonances for which the α-particle widths are determined from the known ^{17}O analog states with a factor uncertainty of 2.5. The ^{13}N$(\alpha, p)^{16}$O reaction rate from Caughlan and Fowler [20] is represented by the green curve and is within a factor of three of the recommended rate across all the temperature range and within less than a factor of two between $T_9 = 0.4$–1. The ^{13}N$(\alpha, p)^{16}$O reaction rate from the STARLIB library [27] based on Hauser-Feschbach theory is represented as the blue curve. The temperature dependence is somewhat similar to the Caughlan and Fowler rate, but the STARLIB rate is systematically lower. For the temperature range of interest, $T_9 = 0.4$–1, the STARLIB rate is lower than the recommended ^{13}N$(\alpha, p)^{16}$O reaction rate from the present work by a factor two.

The fractional contribution of individual resonances to the ^{13}N$(\alpha, p)^{16}$O reaction rate is represented in Fig. 8. Three resonances at $E_r^{\text{c.m.}} = 221$, 741, and 959 keV are dominating the ^{13}N$(\alpha, p)^{16}$O reaction rate, the latter being the major contributor in the temperature range of interest $T_9 = 0.4$–1. While at $T_9 = 0.4$ the ^{13}N$(\alpha, p)^{16}$O reaction rate is mostly dominated by the single resonance at 741 keV, several resonances contribute at $T_9 = 1$. The case of the $E_r^{\text{c.m.}} = 959$ keV resonance is interesting since its relative contribution can be consistent with zero or as high as 60% at $T_9 = 1$. The broad resonance at 1664 keV may contribute across all the temperature range of interest because of its large natural width ($\Gamma = 795$ keV).

In this work resonances up to an energy of 2.4 MeV are considered. This corresponds to a cutoff temperature of 1.4 GK when the procedure relying on the cumulative distribution of fractional resonant rates given in Ref. [57] is followed. Below this temperature the low, rec-

ommended, and high ^{13}N(α, p) ^{16}O reaction rates come from the present Monte Carlo study. At higher temperatures the recommended reaction rate is calculated by normalizing the ^{13}N(α, p) ^{16}O Hauser-Feshbach reaction rate given in the STARLIB database [27]. The reaction rates are given numerically in Table III.

C. Discussion

The main source of uncertainty for the ^{13}N(α, p) ^{16}O reaction rate comes from the 2.5 factor associated to the α-particle widths uncertainty for resonances having a known ^{17}O analog state. This is particularly true for the $E_r^{\mathrm{c.m.}} = 221$ keV ($E_x = 6.039$ MeV) and 741 keV ($E_x = 6.560$ MeV) resonances in the $T_9 = 0.4$–1 range. Reducing these uncertainties should be the first priority for future dedicated experimental work. The remaining uncertainty are caused by the unknown spins and parities together with the large correlated energy uncertainty. Additional Monte Carlo reaction rate calculations have been performed assuming smaller uncertainties for the spectroscopic properties (spin-parity, energy, partial widths) of the $\alpha + {}^{13}$N resonances. These calculations show a reduction of the uncertainty on the ^{13}N(α, p) ^{16}O reaction rate but the recommended rate does not vary by more than 10%. Similarly, the effect of the uncertainty on the θ_α^2 parameter has been investigated considering two additional cases, e.g., $\theta_\alpha^2 = 0.03 \pm 0.02$ and $\theta_\alpha^2 = 0.05 \pm 0.02$. As in Ref. [52] we find that the uncertainty on this value has a minor impact on the final recommended ^{13}N(α, p) ^{16}O reaction rate.

Interference effects have been neglected in this work given the current level of uncertainty on the spin and parity, and the resonance strengths, of states within 2.4 MeV above the ^{13}N $+\alpha$ threshold. The level at 6.560 MeV could interfere with the level at 7.753 MeV if its spin-parity assignment ($1/2^+$) is confirmed. However, the effect of either constructive or destructive interferences would be hindered by the contribution of the broad 7.483-MeV state. The case of interfering $3/2^+$ states is different since the broad 7.483-MeV state ($\Gamma_{\mathrm{tot}} = 795$ keV) can interfere with the two potential $3/2^+$ states at 6.778 and 7.361 MeV. The impact of these interferences would be most noticeable between the two levels at 6.778 and 7.361 MeV, well within the Gamow energy window for $T_9 = 1$. At lower energies, below the 6.778 MeV state, interference effects would be obscured by the 6.560 MeV contribution. Reaction rate calculations of the cases discussed above have shown that the interference effects account for at most a few-percent change in the recommended reaction rate.

The contribution to the reaction rate of the states at $E_x = 7.452, 7.459, 7.476, 7.951$ and 8.017 MeV has not been taken into account since their spins and parities are not known. However their impact has been estimated assuming these states have $J^\pi = 1/2^-$ ($\ell_\alpha = 0$) and a dimensionless reduced α-particle width $\theta_\alpha^2 = 0.04$. $\mathcal{R}$-matrix calculations show that none of these resonances can contribute significantly for $T_9 \leqslant 1$, and therefore they can be safely neglected in this temperature regime. This situation arises from the rather small total width of these resonances ($\sim$5–50 keV) located at energies

TABLE III. Low, recommended, and high thermonuclear rates of the ^{13}N(α, p) ^{16}O reaction are given in cm^3 s^{-1} mol^{-1} as a function of temperature (T_9). Rates are derived from a Monte Carlo approach below the cutoff temperature ($T_9 = 1.4$) (see text) and come from the STARLIB database at higher temperatures.

T_9	Low	Recommended	High
0.01	8.63×10^{-55}	3.07×10^{-54}	1.25×10^{-53}
0.011	1.48×10^{-52}	5.15×10^{-52}	2.06×10^{-51}
0.012	1.41×10^{-50}	4.77×10^{-50}	1.89×10^{-49}
0.013	8.25×10^{-49}	2.73×10^{-48}	1.07×10^{-47}
0.014	3.23×10^{-47}	1.06×10^{-46}	4.10×10^{-46}
0.015	9.09×10^{-46}	2.93×10^{-45}	1.12×10^{-44}
0.016	1.93×10^{-44}	6.13×10^{-44}	2.30×10^{-43}
0.018	4.32×10^{-42}	1.33×10^{-41}	4.81×10^{-41}
0.02	4.57×10^{-40}	1.36×10^{-39}	4.78×10^{-39}
0.025	5.25×10^{-36}	1.44×10^{-35}	4.77×10^{-35}
0.03	6.77×10^{-33}	1.74×10^{-32}	5.31×10^{-32}
0.04	2.46×10^{-28}	5.85×10^{-28}	1.54×10^{-27}
0.05	5.16×10^{-25}	1.16×10^{-24}	2.70×10^{-24}
0.06	2.23×10^{-22}	4.99×10^{-22}	1.12×10^{-21}
0.07	3.16×10^{-20}	7.05×10^{-20}	1.60×10^{-19}
0.08	1.73×10^{-18}	3.89×10^{-18}	8.83×10^{-18}
0.09	4.43×10^{-17}	1.00×10^{-16}	2.29×10^{-16}
0.1	6.35×10^{-16}	1.44×10^{-15}	3.29×10^{-15}
0.11	5.92×10^{-15}	1.32×10^{-14}	3.02×10^{-14}
0.12	3.93×10^{-14}	8.69×10^{-14}	1.98×10^{-13}
0.13	2.03×10^{-13}	4.42×10^{-13}	1.00×10^{-12}
0.14	8.66×10^{-13}	1.86×10^{-12}	4.15×10^{-12}
0.15	3.19×10^{-12}	6.69×10^{-12}	1.46×10^{-11}
0.16	1.05×10^{-11}	2.13×10^{-11}	4.56×10^{-11}
0.18	8.73×10^{-11}	1.67×10^{-10}	3.33×10^{-10}
0.2	5.52×10^{-10}	1.01×10^{-09}	1.93×10^{-09}
0.25	2.70×10^{-08}	4.75×10^{-08}	8.57×10^{-08}
0.3	6.43×10^{-07}	1.13×10^{-06}	2.09×10^{-06}
0.35	9.13×10^{-06}	1.64×10^{-05}	3.19×10^{-05}
0.4	8.64×10^{-05}	1.59×10^{-04}	3.17×10^{-04}
0.45	5.88×10^{-04}	1.10×10^{-03}	2.21×10^{-03}
0.5	3.03×10^{-03}	5.70×10^{-03}	1.15×10^{-02}
0.6	4.20×10^{-02}	8.15×10^{-02}	1.65×10^{-01}
0.7	3.15×10^{-01}	6.14×10^{-01}	$1.26 \times 10^{+00}$
0.8	$1.57 \times 10^{+00}$	$3.00 \times 10^{+00}$	$6.24 \times 10^{+00}$
0.9	$5.94 \times 10^{+00}$	$1.10 \times 10^{+01}$	$2.29 \times 10^{+01}$
1	$1.82 \times 10^{+01}$	$3.30 \times 10^{+01}$	$6.65 \times 10^{+01}$
1.25	$1.67 \times 10^{+02}$	$2.84 \times 10^{+02}$	$5.17 \times 10^{+02}$
1.5	$8.66 \times 10^{+02}$	$1.41 \times 10^{+03}$	$2.37 \times 10^{+03}$
1.75	$2.88 \times 10^{+03}$	$4.68 \times 10^{+03}$	$7.86 \times 10^{+03}$
2	$9.55 \times 10^{+03}$	$1.55 \times 10^{+04}$	$2.61 \times 10^{+04}$
2.5	$4.88 \times 10^{+04}$	$7.95 \times 10^{+04}$	$1.34 \times 10^{+05}$
3	$1.62 \times 10^{+05}$	$2.63 \times 10^{+05}$	$4.42 \times 10^{+05}$
3.5	$4.06 \times 10^{+05}$	$6.61 \times 10^{+05}$	$1.11 \times 10^{+06}$
4	$8.48 \times 10^{+05}$	$1.38 \times 10^{+06}$	$2.32 \times 10^{+06}$
5	$2.57 \times 10^{+06}$	$4.19 \times 10^{+06}$	$7.04 \times 10^{+06}$
6	$5.76 \times 10^{+06}$	$9.37 \times 10^{+06}$	$1.57 \times 10^{+07}$
7	$1.06 \times 10^{+07}$	$1.73 \times 10^{+07}$	$2.91 \times 10^{+07}$
8	$1.72 \times 10^{+07}$	$2.80 \times 10^{+07}$	$4.71 \times 10^{+07}$
9	$2.54 \times 10^{+07}$	$4.13 \times 10^{+07}$	$6.95 \times 10^{+07}$
10	$3.49 \times 10^{+07}$	$5.68 \times 10^{+07}$	$9.55 \times 10^{+07}$

well above the upper bound of the Gamow peak for $T_9 = 1$ ($E = 1.375$ MeV).

V. ASTROPHYSICAL IMPLICATIONS

To understand the impact of the new rate of the ^{13}N$(\alpha, p)^{16}$O reaction, we have performed single-zone post-processing nucleosynthesis simulations. Sixteen explosive trajectories including temperature and densities evolving over time were extracted from the He shell of the 15 $M_\odot$, metallicity $(Z) = 0.02$ core-collapse supernova (CCSN) model in Ref. [58]. These trajectories are representative of a range of 0.4 GK $\lesssim T \lesssim 0.7$ GK for the peak temperature at the passage of the SN shock. For the initial abundances, we used the He shell pre-explosive composition between mass coordinates 6.95 $M_\odot$ and 7.05 $M_\odot$ from the 25 $M_\odot$, $Z = 0.02$ massive star model in Ref. [59], following the same approach used in Ref. [15]. In particular, it is relevant to use this initial composition since the 25 $M_\odot$ stellar model experienced H ingestion in the He shell, and therefore its abundance signature will be representative for the impact study provided in this work. The He-rich shell material is left with about 1.2 % of H.

The post-SN abundances have been calculated using the PPN NuGrid Post-Processing Nucleosynthesis code [59] with the following nuclear network setup. We used 5195 species (from H to Bi, including all the unstable isotopes by β decay with a half-life longer than 10^{-5} s) and 66 953 reactions. We refer to Ref. [59] for a detailed list of all nuclear rates used in the network. For each trajectory, we ran three sets of simulations using the ^{13}N$(\alpha, p)^{16}$O reaction rate from CF88 compilation, and the CF88 rate divided and multiplied by a factor of five. The isotopic abundances profiles for the stable isotopes H, ^{4}He, ^{12}C, ^{13}C, ^{14}N, ^{15}N, and ^{16}O, including the decay of unstable species, and for the short-lived isotopes ^{22}Na and ^{26}Al are shown in Fig. 9 (upper panel). These are the same calculation as performed in Fig. 1, but using a set of explosive He-burning trajectories that covers the complete range of relevant temperature conditions, as described above. Therefore the results obtained in Fig. 9 are consistent with Fig. 1, since the stellar conditions in the two calculations are the same. The only apparent difference is that while simulations based on mass coordinate refer to the specific progenitor model used, the calculations shown in Fig. 1 are representative of explosive He-burning conditions independently of the original model. Therefore, the abundance profiles with respect to the SN peak temperatures is comparable to nucleosynthesis results shown with respect to mass coordinate from any model of CCSN explosive He-burning layers. We then performed a second set of calculations, using the low and the high thermonuclear reaction rates, from the present work, given in Table III. For comparison, the abundances obtained using these rates are shown in Fig. 9 (lower panel).

In both cases, the largest impact of the ^{13}N$(\alpha, p)^{16}$O reaction rate on ^{13}C abundances is for a peak temperature of 0.54 GK. As expected the largest abundance variation decreases when the rates from the present work are used. Furthermore, the temperature range where the ^{13}N$(\alpha, p)^{16}$O reaction rate has an impact is also reduced. With the ^{13}N$(\alpha, p)^{16}$O
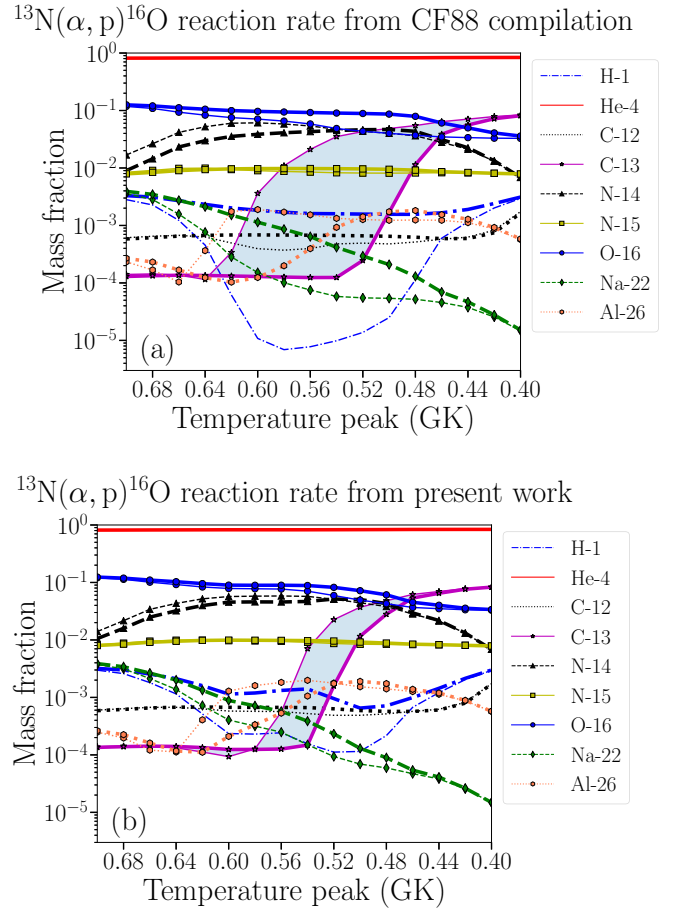

FIG. 9. Isotopic abundances in the He-shell ejecta of a 25 $M_\odot$ supernova model. Upper panel: Impact of a variation of the ^{13}N$(\alpha, p)^{16}$O reaction rate by an arbitrary factor of five with respect to the CF88 rate. Thick (thin) lines correspond to a variation of the rate by a factor of five up (down), respectively. Lower panel: Impact of the ^{13}N$(\alpha, p)^{16}$O reaction rate from present work when the upper and lower limits of the rate are used (thick and thin lines, respectively). In both panels the uncertainty range for ^{13}C abundances is highlighted in light blue.

reaction rates from the present work the uncertainty on the integrated ^{13}C yield, highlighted in light blue in Fig. 9 (bottom), is a factor of 7 for the lower and the upper limit compared to the adopted rate. This will improve future theoretical predictions of ^{13}C production in CCSN models with H ingestion.

Figure 10 also illustrates the largest impact of the ^{13}N$(\alpha, p)^{16}$O reaction rate from the present work on production factors of stable isotopes, including the decay of unstable species, in the mass region between ^{12}C and ^{50}V, using the trajectory with the temperature peak of 0.54 GK. From Fig. 10 it is interesting to notice the strong impact of the ^{13}N$(\alpha, p)^{16}$O rate in making ^{13}C and ^{17}O during the SN shock, where the reaction is reducing the radiogenic production of ^{13}C from the ^{13}N decay, and favors the nucleosynthesis flow passing via ^{17}O. If we consider ^{17}O for instance, then a higher ^{13}N$(\alpha, p)^{16}$O rate would increase the abundance of ^{16}O, which increases the ^{16}O$(p, \gamma)^{17}$F rate, feeding the radiogenic production of ^{17}O. In the same way, a
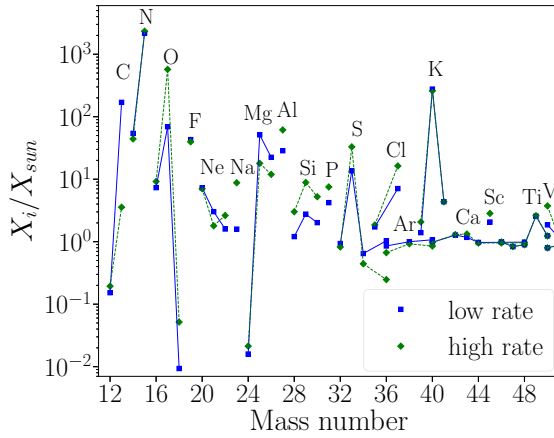
FIG. 10. Production factors of stable isotopes, including the decay of unstable species, in the mass region between ^{12}C and ^{50}V, obtained using the lower limit of the ^{13}N(α, p)^{16}O reaction rate from present work (blue squares) and the upper limit (green diamonds) from the trajectory with temperature peak of the SN shock of 0.54 GK. Isotopes of a given element are connected with lines.

higher ^{13}N(α, p)^{16}O rate also increases the amount of protons available to be captured, which also increases the proton capture rate on ^{16}O. Together with ^{13}C and ^{17}O, we find that other species affected in the He shell are between ^{23}Na and ^{37}Cl. This is due again to the impact that the ^{13}N(α, p)^{16}O reaction has on the α-particle and proton budget during the SN explosion. Isotopes of the intermediate-mass elements are also produced in deeper layers of the SN ejecta, and their enhanced production in the He shell cannot be disentangled, to allow comparison with observations.

Novae and fast-rotating massive stars have been proposed as important stellar sources for ^{13}C, ^{15}N, and ^{17}O (e.g., Refs. [60,61] and references therein), but a clear picture is not yet defined. References [15] discussed the possible impact in contributing to the galactic chemical evolution of ^{15}N. The H ingestion in He shell layers and following nucleosynthesis in the SN shock may therefore have a strong impact on the overall production of these H-burning products. For more robust predictions for the final abundance of ^{13}C, ^{15}N, and ^{17}O in the type of models discussed in this work, the support of multidimensional hydrodynamics models is required (see discussion in Ref. [15]).

VI. SUMMARY AND CONCLUSIONS

A new ^{13}N(α, p)^{16}O reaction rate with meaningful statistical uncertainty has been evaluated using the most up to date ^{17}F spectroscopic information. First, the FR-DWBA analysis of the ^{13}C(^{7}Li, t)^{17}O transfer reaction populating ^{17}O states (analog of ^{17}F states) in the $E_x = 5.6$–7.8 MeV range has been reported. The α-particle spectroscopic factors were extracted and the deduced α-particle widths were found to be within a factor of two of reported values in the literature when

available. The α-particle spectroscopic factors were then used to deduce α-particle widths of ^{17}F analog states when the mirror connection with ^{17}O levels could be established. If not, then assumption on the dimensionless α-particle reduced widths was used ($\langle\theta_\alpha^2\rangle = 0.04$).

A Monte Carlo procedure consistently taking into account uncertainties on the energy, partial/total width and spin and parity of the ^{17}F states was then used to determine the ^{13}N(α, p)^{16}O reaction rate and its corresponding statistical uncertainty. Correlation effects for the energy uncertainty of ^{17}F states has been taken into account in the present work when needed. The ^{13}N(α, p)^{16}O nominal rate is consistent within a factor of two with previous rate [20] used in stellar models, and its uncertainty in the temperature range of interest is $\approx$2. It has been shown that the main uncertainty in the reaction rate comes from the uncertainty associated to the α-particle width of ^{17}F states. In order to improve this situation an experimental determination of the α-particle widths of unbound ^{17}F states should be a priority.

The new ^{13}N(α, p)^{16}O reaction rate and corresponding uncertainty has been used to study the nucleosynthesis in 16 explosive He-burning trajectories, with temperature peaks ranging between 0.4 and 0.7 GK, from state-of-the-art CCSN stellar models. The abundance signature of proton ingestion in the He layer of the massive stars progenitor is considered. Results show that with the present rates the uncertainty on the ^{13}C integrated yield from these models is about a factor of 50 when using the lower and upper reaction rates. Future stellar yields of CNO isotopes from CCSNe models including H ingestion will definitely need to consider the ^{13}N(α, p)^{16}O reaction.

[1] J. Yoon, T. C. Beers, S. Dietz, Y. S. Lee, V. M. Placco, G. Da Costa, S. Keller, C. I. Owen, and M. Sharma, Astrophys. J. **861**, 146 (2018).

[2] B. K. Gibson, Y. Fenner, A. Renda, D. Kawata, and H.-c. Lee, Publ. Astron. Soc. Austr. **20**, 401 (2003).

[3] C. Kobayashi, A. I. Karakas, and H. Umeda, Mon. Not. Roy. Astron. Soc. **414**, 3231 (2011).

[4] T. Mishenina, M. Pignatari, B. Côté, F.-K. Thielemann, C. Soubiran, N. Basak, T. Gorbaneva, S. A. Korotin, V. V. Kovtyukh, B. Wehmeyer, S. Bisterzo, C. Travaglio, B. K. Gibson, C. Jordan, A. Paul, C. Ritter, F. Herwig, and NuGrid Collaboration, Mon. Not. Roy. Astron. Soc. **469**, 4378 (2017).

[5] B. W. Grefenstette, F. A. Harrison, S. E. Boggs, S. P. Reynolds, C. L. Fryer, K. K. Madsen, D. R. Wik, A. Zoglauer, C. I. Ellinger, D. M. Alexander, H. An, D. Barret, F. E. Christensen, W. W. Craig, K. Forster, P. Giommi, C. J. Hailey, A. Hornstrup, V. M. Kaspi, T. Kitaguchi, J. E. Koglin, P. H. Mao, H. Miyasaka, K. Mori, M. Perri, M. J. Pivovaroff, S. Puccetti, V. Rana, D. Stern, N. J. Westergaard, and W. W. Zhang, Nature **506**, 339 (2014).

[6] H. Yamaguchi, C. Badenes, A. R. Foster, E. Bravo, B. J. Williams, K. Maeda, M. Nobukawa, K. A. Eriksen, N. S. Brickhouse, R. Petre, and K. Koyama, Astrophys. J. Lett. **801**, L31 (2015).

[7] E. Zinner, Presolar grains, in *Meteorites and Cosmochemical Processes*, Volume 1 of Treatise on Geochemistry, edited by A. M. Davis (Elsevier, 2014), pp. 181–213, 2nd ed.

[8] M. Pignatari, M. Wiescher, F. X. Timmes, R. J. de Boer, F.-K. Thielemann, C. Fryer, A. Heger, F. Herwig, and R. Hirschi, Astrophys. J. Lett. **767**, L22 (2013).

[9] A. Besmehn and P. Hoppe, Geochimica et Cosmochimica Acta **67**, 4693 (2003).

[10] M. Pignatari, E. Zinner, M. G. Bertolli, R. Trappitsch, P. Hoppe, T. Rauscher, C. Fryer, F. Herwig, R. Hirschi, F. X. Timmes, and F.-K. Thielemann, Astrophys. J. Lett. **771**, L7 (2013).

[11] S. Amari, A. Anders, A. Virag, and E. Zinner, Nature **345**, 238 (1990).

[12] L. R. Nittler and P. Hoppe, Astrophys. J. Lett. **631**, L89 (2005).

[13] J. José and M. Hernanz, J. Phys. G Nucl. Phys. **34**, R431 (2007).

[14] P. A. Denissenkov, J. W. Truran, M. Pignatari, R. Trappitsch, C. Ritter, F. Herwig, U. Battino, K. Setoodehnia, and B. Paxton, Mon. Not. Roy. Astron. Soc. **442**, 2058 (2014).

[15] M. Pignatari, E. Zinner, P. Hoppe, C. J. Jordan, B. K. Gibson, R. Trappitsch, F. Herwig, C. Fryer, R. Hirschi, and F. X. Timmes, Astrophys. J. Lett. **808**, L43 (2015).

[16] R. J. Stancliffe, D. S. P. Dearborn, J. C. Lattanzio, S. A. Heap, and S. W. Campbell, Astrophys. J. **742**, 121 (2011).

[17] F. Herwig, P. R. Woodward, P.-H. Lin, M. Knox, and C. Fryer, Astrophys. J. Lett. **792**, L3 (2014).

[18] P. A. Denissenkov, F. Herwig, P. Woodward, R. Andrassy, M. Pignatari, and S. Jones, Mon. Not. Roy. Astron. Soc. **488**, 4258 (2019).

[19] O. Clarkson, F. Herwig, R. Andrassy, P. Woodward, M. Pignatari, and H. Mao, in *Nuclei in the Cosmos XV*, Springer Proceedings in Physics, Vol. 219, edited by A. Formicola, M. Junker, L. Gialanella, and G. Imbriani (Springer, Cham, 2019), pp. 321–325.

[20] G. R. Caughlan and W. A. Fowler, At. Data Nucl. Data Table **40**, 283 (1988).

[21] S. Takács, F. Tárkányi, A. Hermanne, and R. Paviotti de Corcuera, Nuclear Instrum. Methods B **211**, 169 (2003).

[22] A. V. Nero and A. J. Howard, Nucl. Phys. A **210**, 60 (1973).

[23] W. Gruhle and B. Kober, Nucl. Phys. A **286**, 523 (1977).

[24] R. V. Wagoner, W. A. Fowler, and F. Hoyle, Astrophys. J. **148**, 3 (1967).

[25] R. V. Wagoner, Astrophys. J. Supp. **18**, 247 (1969).

[26] J. N. Bahcall, Astrophys. J. **143**, 259 (1966).

[27] A. L. Sallaska, C. Iliadis, A. E. Champange, S. Goriely, S. Starrfield, and F. X. Timmes, Astrophys. J. Supp. **207**, 18 (2013).

[28] D. R. Tilley, H. R. Weller, and C. M. Cheves, Nucl. Phys. A **564**, 1 (1993).

[29] M. G. Pellegriti, F. Hammache, P. Roussel, L. Audouin, D. Beaumel, P. Descouvemont, S. Fortier, L. Gaudefroy, J. Kiener, A. Lefebvre-Schuhl, M. Stanoiu, V. Tatischeff, and M. Vilmay, Phys. Rev. C **77**, 042801 (2008).

[30] J. E. Spencer and H. A. Enge, Nuclear Instrum. Methods **49**, 181 (1967).

[31] R. G. Markham and R. G. Robertson, Nuclear Instrum. Methods **129**, 131 (1975).

[32] C. H. Johnson, Phys. Rev. C **7**, 561 (1973).

[33] D. Lister and A. Sayres, Phys. Rev. **143**, 745 (1966).

[34] T. Faestermann, P. Mohr, R. Hertenberger, and H.-F. Wirth, Phys. Rev. C **92**, 052802 (2015).

[35] I. J. Thompson, Comput. Phys. Rep. **7**, 167 (1988).

[36] N. de Séréville, A. Meyer, F. Hammache, A. M. Laird, and M. Pignatari, in *Nuclear Physics in Astrophysics VIII (NPA8 2017)*, EPJ Web of Conferences, Vol. 165, edited by M. La Cognata *et al.* (EDP Sciences, 2017), p. 285.

[37] P. Schumacher, N. Ueta, H. H. Duhm, K.-I. Kubo, and W. J. Klages, Nucl. Phys. A **212**, 573 (1973).

[38] J. D. Garrett and O. Hansen, Nucl. Phys. A **212**, 600 (1973).

[39] M. Moshinsky, Nucl. Phys. A **13**, 104 (1959).

[40] G. E. Brown and A. M. Green, Nucl. Phys. **75**, 401 (1966).

[41] F. D. Becchetti, E. R. Flynn, D. L. Hanson, and J. W. Sunier, Nucl. Phys. A **305**, 293 (1978).

[42] C. Iliadis, *Nuclear Physics of Stars* (Wiley-VCH, Verlag GmbH & Co. KGaA, Weinheim, Germany, 2008).

[43] M. Heil, R. Detwiler, R. E. Azuma, A. Couture, J. Daly, J. Görres, F. Käppeler, R. Reifarth, P. Tischhauser, C. Ugalde, and M. Wiescher, Phys. Rev. C **78**, 025803 (2008).

[44] R. O. Sayer, L. C. Leal, N. M. Larson, R. R. Spencer, and R. Q. Wright, R-matrix evaluation of ^{16}O neutron cross sections up to 6.3 MeV, Technical Report ORNL/TM-2000/212 (2000) (unpublished).

[45] S. R. Salisbury, G. Hardie, L. Oppliger, and R. Dangle, Phys. Rev. **126**, 2143 (1962).

[46] S. R. Salisbury and H. T. Richards, Phys. Rev. **126**, 2147 (1962).

[47] R. L. Dangle, L. D. Oppliger, and G. Hardie, Phys. Rev. **133**, B647 (1964).

[48] W. J. Huang, G. Audi, M. Wang, F. G. Kondev, S. Naimi, and X. Xu, Chin. Phys. C **41**, 030002 (2017).

[49] F. Ajzenberg-Selove, Nucl. Phys. A **460**, 1 (1986).

[50] F. de Oliveira, A. Coc, P. Aguer, G. Bogaert, J. Kiener, A. Lefebvre, V. Tatischeff, J.-P. Thibaud, S. Fortier, J. M. Maison, L. Rosier, G. Rotbard, J. Vernotte, S. Wilmes, P. Mohr, V. Kölle, and G. Staudt, Phys. Rev. **55**, 3149 (1997).

[51] D. E. Alburger and D. H. Wilkinson, Phys. Rev. C **13**, 835 (1976).

[52] P. Mohr, R. Longland, and C. Iliadis, Phys. Rev. C **90**, 065806 (2014).

[53] I. Pogrebnyak, C. Howard, C. Iliadis, R. Longland, and G. E. Mitchell, Phys. Rev. C **88**, 015808 (2013).

[54] R. E. Azuma, E. Uberseder, E. C. Simpson, C. R. Brune, H. Costantini, R. J. de Boer, J. Görres, M. Heil, P. J. Leblanc, C. Ugalde, and M. Wiescher, Phys. Rev. C **81**, 045805 (2010).

[55] R. Longland, C. Iliadis, A. E. Champagne, J. R. Newton, C. Ugalde, A. Coc, and R. Fitzgerald, Nucl. Phys. A **841**, 1 (2010).

[56] R. Longland, Astron. Astrophys. **604**, A34 (2017).

[57] J. R. Newton, R. Longland, and C. Iliadis, Phys. Rev. C **78**, 025805 (2008).

[58] C. L. Fryer, S. Andrews, W. Even, A. Heger, and S. Safi-Harb, Astrophys. J. **856**, 63 (2018); S. Jones and C. Fryer (private communication).

[59] M. Pignatari, F. Herwig, R. Hirschi, M. Bennett, G. Rockefeller, C. Fryer, F. X. Timmes, C. Ritter, A. Heger, S. Jones, U. Battino, A. Dotter, R. Trappitsch, S. Diehl, U. Frischknecht, A. Hungerford, G. Magkotsios, C. Travaglio, and P. Young, Astrophys. J. Suppl. **225**, 24 (2016).

[60] D. Romano, F. Matteucci, Z.-Y. Zhang, R. J. Ivison, and P. Ventura, Mon. Not. Roy. Astron. Soc. **490**, 2838 (2019).

[61] C. Chiappini, S. Ekström, G. Meynet, R. Hirschi, A. Maeder, and C. Charbonnel, Astron. Astrophys. **479**, L9 (2008).